Supporting Information

Multiangular Rod-Shaped $Na_{0.44}MnO_2$ as Cathode Materials with High Rate and Long Life for Sodium-Ion Batteries

Qiannan Liu,[†] Zhe Hu,[†] Mingzhe Chen,[†] Qinfen Gu,[*, ‡] Yuhai Dou,[†] Ziqi Sun,[*, §] Shulei Chou,[*, †] and Shi Xue Dou[†]

[†] Institute for Superconducting and Electronic Materials, Australian Institute for Innovative Materials, University of Wollongong, Innovation Campus, Squires Way, North Wollongong, NSW 2522, Australia

[‡] Australian Synchrotron, 800 Blackburn Road, Clayton, VIC 3168, Australia

[§] School of Chemistry, Physics and Mechanical Engineering, Queensland University of Technology, Gardens Point, Brisbane, QLD 4000, Australia

Corresponding authors:
E-mail addresses: qinfen.gu@synchrotron.org.au (Q.G.); ziqi.sun@qut.edu.au (Z.S.); shulei@uow.edu.au (S.C.).

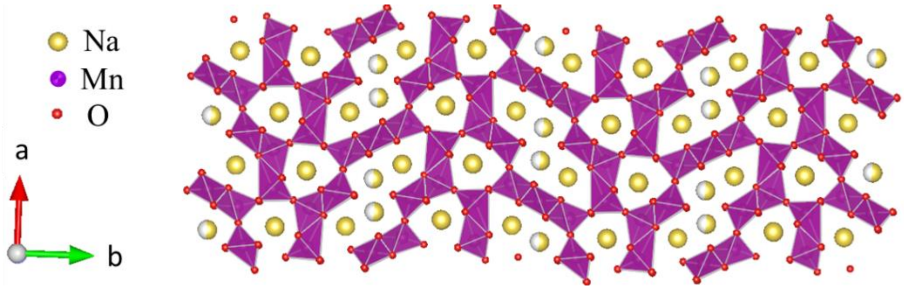

Figure S1. Schematic crystal structure of orthorhombic $Na_{0.44}MnO_2$.

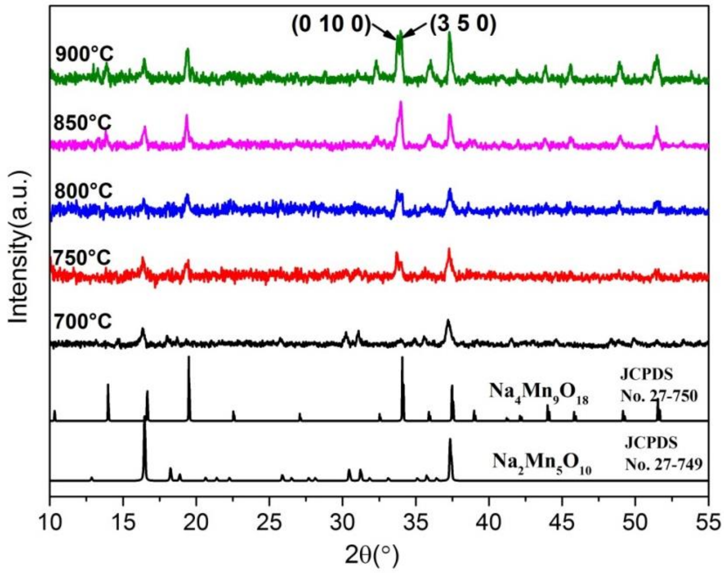

Figure S2. X-ray diffraction patterns collected with Cu K_{α} radiation of powders calcined at different temperatures.

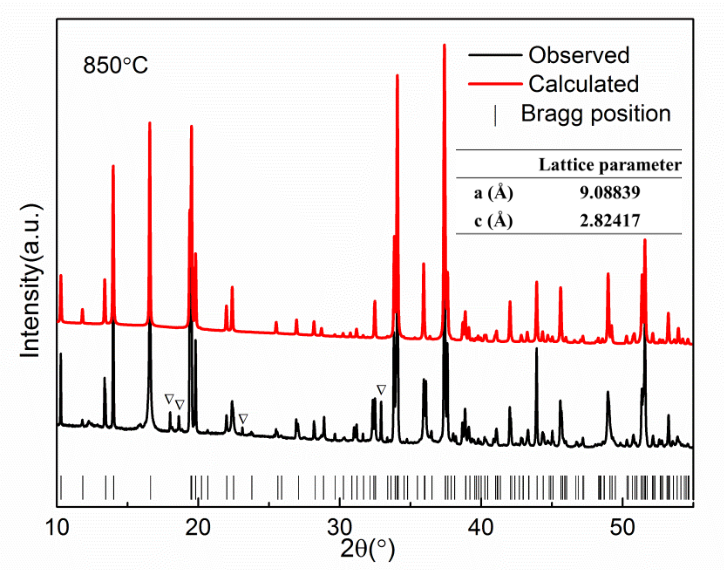

Figure S3. XRD pattern and lattice parameter of Rietveld refinement of NMO850. The peaks marked with ∇ are unknown impurities.

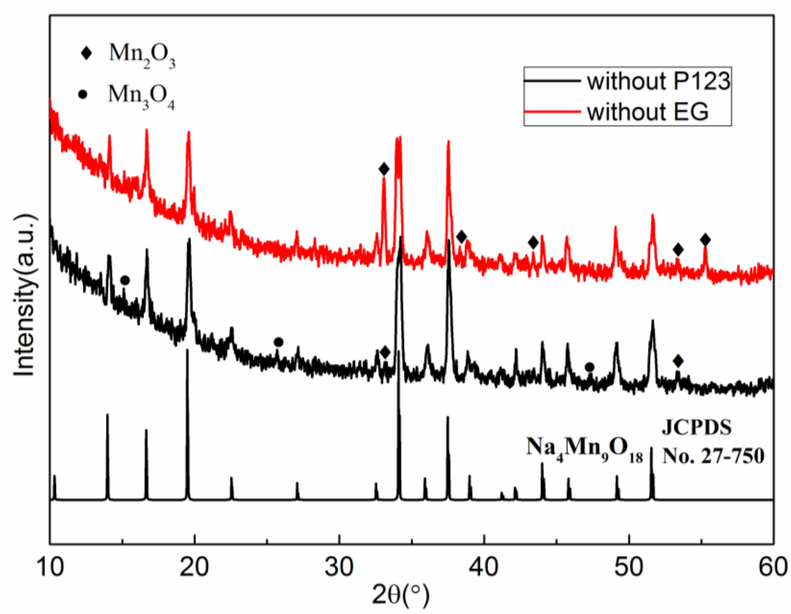

Figure S4. Laboratory X-ray diffraction patterns collected with Cu K_α radiation of NMO850 without the addition of P123 or EG.

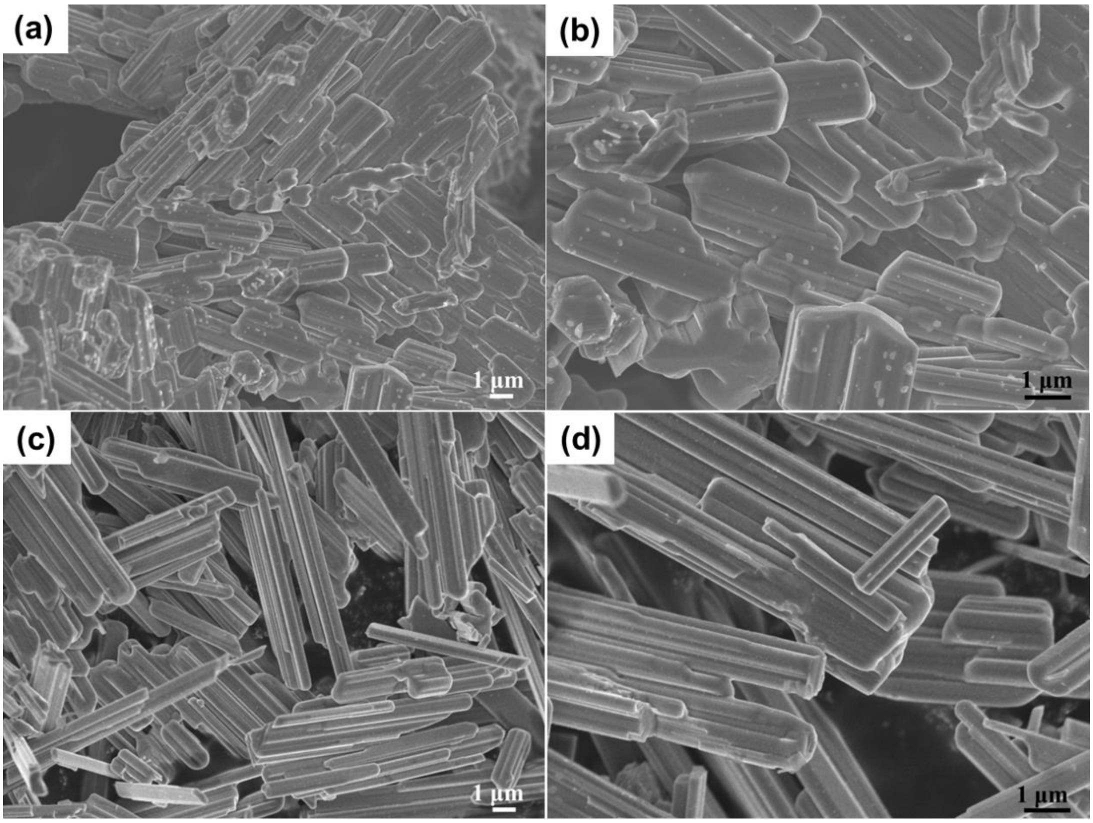

Figure S5. SEM morphologies of NMO850 without the addition of P123: (a) low magnification, (b) high magnification; and without the addition of EG: (c) low magnification, (d) high magnification.

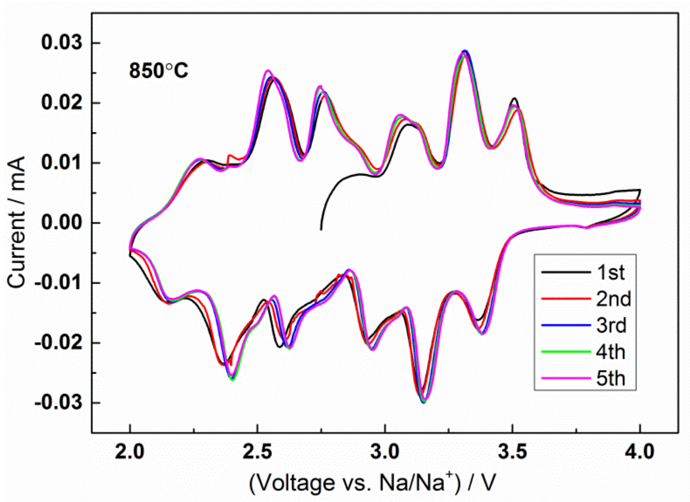

Figure S6. Cyclic voltammograms (CV) of NMO850 for the first five cycles at a scan rate of 0.1 mV s^{-1} in the potential window of 4.0-2.0 V.

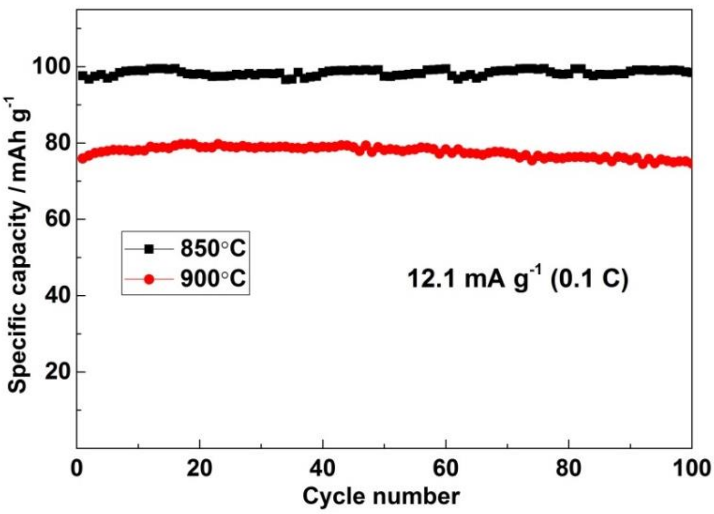

Figure S7. Cycling performance of NMO850 and NMO900 between 3.8-2.0 V at a current density of 12.1 mA g^{-1} (0.1 C).

Figure S7 shows the cycling performance of NMO850 and NMO900 between 3.8-2.0 V at 0.1 C. Both the samples exhibit good cycling performance at 0.1 C, especially NMO850, the discharge capacity of which increases gradually during the 100 cycles. In detail, NMO850 and NMO900 delivered initial discharge capacities of 97.6, and 77.2 mAh g^{-1} in the first cycle, respectively. After an activation process, NMO850 retains a discharge capacity of 99.1 mAh g^{-1} over 100 cycles, corresponding to capacity retention of 101.5% of the initial discharge capacity.

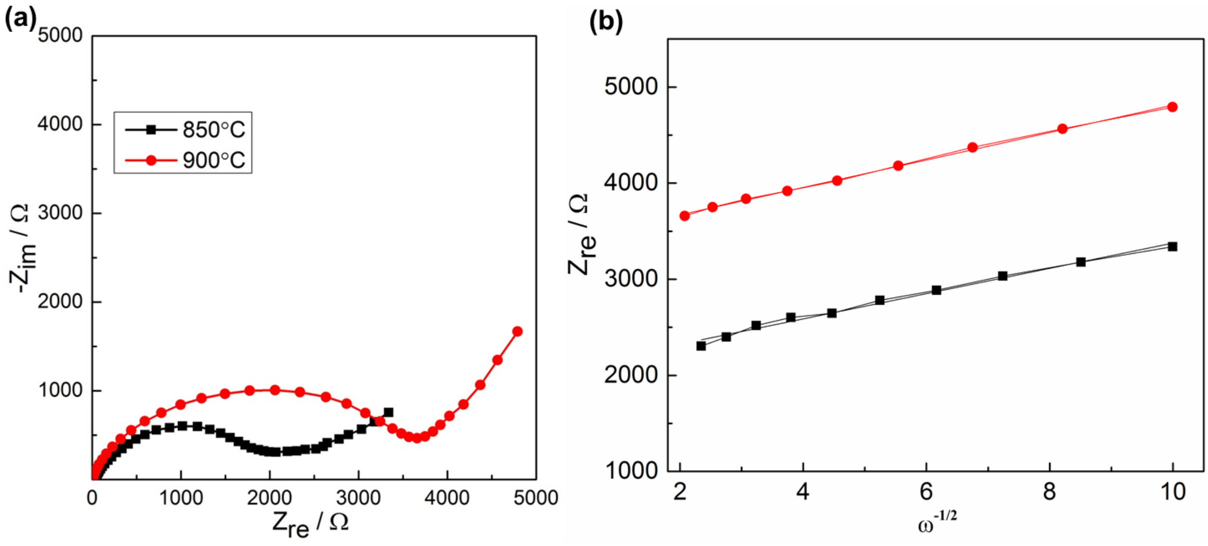

Figure S8. (a) Nyquist plots of NMO850 and NMO900 from 100 kHz to 100 mHz at open circuit potential; and (b) corresponding Z_{re} vs. $\omega^{-1/2}$ plots for the low-frequency region of NMO850 and NMO900.

Figure S8 shows the Nyquist plot of NMO850 and NMO900 at open circuit potential and corresponding Z_{re} vs. $\omega^{-1/2}$ plots of the low-frequency region. Both the samples show a semicircle in the high frequency area and a sloping line in the low frequency region. The depressed semicircle in the high frequency region is attributed to the charge transfer resistance, which is smaller for NMO850, indicating its faster speed of electron transfer compared toNMO900. Through linear fitting of the Z_{re} vs. $\omega^{-1/2}$ plot in the low-frequency region in Figure S8b, the apparent diffusion coefficient of the Na^+ ions at open circuit potential can be calculated to be 2.40×10^{-14} and 1.90×10^{-14} cm^2 s^{-1} for NMO850 and NMO900, respectively, which is consistent with the GITT results in Figure 5.